Available online at www.sciencedirect.com
ScienceDirect
Trans. Nonferrous Met. Soc. China 30(2020) 2848−2860
Transactions of Nonferrous Metals Society of China
www.tnmsc.cn

Effect of rutile crystal shapes on its settlement

Ji-qing HAN[1], Jia-hao ZHANG[1], Xiao CHEN[2], Jing ZHANG[1], Li ZHANG[1], Gan-feng TU[1]

1. School of Metallurgy, Northeastern University, Shenyang 110819, China;
2. School of Materials Science and Engineering, Northeastern University, Shenyang 110819, China

Received 26 December 2019; accepted 5 August 2020

Abstract: The effect of rutile crystal shapes on its settlement in a modified slag was studied by theoretical analysis, FactSage simulation, X-ray diffraction and scanning electron microscopy. The results show that the settling velocities of spherical rutile crystals are faster than those of other shapes of rutile crystals under the same volume conditions, and the shape transformation of rutile crystals from rod to sphere can be achieved by adding titanium slag to Ti-bearing blast furnace slag. The volume fractions of the rutile crystals in the upper and lower parts of the modified slag are 30% and 71% when the added titanium slag increases to 278 g, indicating that rutile settling is obvious. Due to the rutile settling, half shaker sorting task is saved, and the recovery rate of TiO_2 is significantly increased. The TiO_2 content of rutile is greater than 93%, and the total content of CaO and MgO is less than 0.4%, meeting the requirements for the raw materials of titanium white in the chloride process.

Key words: rutile crystal shape; Ti-bearing blast furnace slag; titanium slag; modification; shaker sorting; acid leaching

1 Introduction

China is rich in titanium resources, 95% of which are stored in form of vanadium−titanium magnetite ore in the Southwestern China [1−3]. Currently, vanadium−titanium magnetite concentrate ore containing approximately 30% Fe, 10% TiO_2, and 0.3% V_2O_5 is smelted by using blast furnaces at Panzhihua Iron and Steel Corporation, China. Most Ti components in the ore are separated from iron and are enriched in the molten slag (22%−25% TiO_2). More than 3 million tons of blast furnace slag is produced yearly in China. In recent years, several methods for treating the slag have been proposed, such as flotation separation, magnetic separation, hydrometallurgical and pyrometallurgical methods [4]. However, the recovery efficiency of Ti components of those methods is relatively low, and thereby the slag has not been fully utilized [5]. The Ti constituents, showing complex interfacial boundaries, distribute dispersedly in various fine-grained (<10 μm) mineral phases in the slag, which introduces difficulties for the recovery of Ti components by traditional separation methods.

Based on the above characteristics of Ti components in the slag, a method, aiming to enrich the Ti components in blast furnace slag into perovskite phase, has been proposed and extensively studied [6]. Many studies [7−14] on enriching the Ti components in blast furnace slag into perovskite are available. However, it has been proved that the as-prepared perovskite phase is difficult to be separated from the bulk slag due to its dendrite structure and little difference in density between perovskite and other phases in the slag. Compared to perovskite, rutile possesses a high added value and high density (4.2−4.3 g/cm^3), which makes it a suitable alternative to perovskite

Foundation item: Project (2015BAB18B00) supported by the National Science and Technology Support Program of China
Corresponding author: Li ZHANG; Tel: +86-24-83687750; E-mail: fantai320@163.com
DOI: 10.1016/S1003-6326(20)65426-7

for enriching the Ti components in the slag.

There are some studies on the selective precipitation and separation of the rutile phase. LI et al [15,16] investigated the crystallization behavior of rutile in the synthesized Ti-bearing blast furnace slag. ZHANG et al [17] studied the crystallization and coarsening kinetics of rutile in the modified Ti-bearing blast furnace slag. ZHANG et al [18,19] studied the extraction of rutile from high-titanium slag by modification-alkali leaching-dilute acid washing or preoxidation-modification-acid leaching method. DU et al [20,21] investigated the selective precipitation and in-situ separation of rutile crystals from titanium-bearing slag melt in a super-gravitational field. In the above works, Ti components were successfully enriched into the rutile phase. However, to date, the rutile settlement in a natural-gravitational field has not been reported.

The objective of this work is to study the effect of rutile crystal shapes on rutile settlement in a modified slag by theoretical analysis, FactSage simulation, X-ray diffraction (XRD), and scanning electron microscopy (SEM). Further, the mechanism of formation of rutile was explained by the standard Gibbs free-energy change of reaction. The rutile settlement can save half the shaker sorting task for the technology and significantly increase the recovery rate of TiO_2.

2 Experimental

2.1 Materials

In this study, Ti-bearing blast furnace slag was purchased from Panzhihua Iron and Steel Research Institute (Sichuan Province, China). Based on previous research [22], titanium slag was prepared from titanium middling ore. The additive, SiO_2, was of analytical grade and provided by China National Medicines Corporation Ltd., O_2, with a purity of 99% (mass fraction), was provided by Shenyang Shuntai Gas Corporation Ltd., China. The chemical compositions of Ti-bearing blast furnace slag and titanium slag are listed in Table 1.

2.2 Experimental procedures

2.2.1 FactSage simulation

The masses of O_2 and SiO_2 for each experiment were calculated by FactSage. The initial chemical components of Ti-bearing blast furnace slag and titanium slag were chosen based on the data listed in Table 1. The Scheil−Gulliver cooling method in the Equilib module of FactSage was used to build the relationships among the added SiO_2, O_2, and rutile precipitation. The cooling temperature range for simulation is 1000−1450 °C. The FToxid and FactPS databases were used in the simulation.

2.2.2 Modified experiments

The modification experiments were performed in a vertical $MoSi_2$ furnace with a B-type thermocouple. It was estimated that the overall absolute temperature accuracy of the experiment was ±3 °C. The oxidation gas was oxygen, and the flow rate of O_2 was regulated by a rotameter.

According to the above-mentioned FactSage simulation results, 500 g of Ti-bearing blast furnace slag and titanium slag as well as a certain addition of SiO_2 were loaded into a crucible under Ar atmosphere at 1450 °C for 20 min to melt them as fully as possible. Then, O_2 was blown into molten slag at a flow rate of 5 L/min under isothermal conditions. Subsequently, the molten slag was slowly cooled to room temperature at a cooling rate of 5 °C/min.

The pilot experiments for 44.4 kg of Ti-bearing blast furnace slag, 55.6 kg of titanium slag, and 8 kg of SiO_2 were conducted in a pilot plant. Under isothermal conditions (1450 °C), O_2 was directly blown into molten slag at a flow rate of 50 L/min, and the temperature was measured by a B-type thermocouple. When the molten slag started to cool from 1450 °C, the central molten slags with cooling time of 6, 10, 14, and 18 min were quenched in water, then the settlement time of rutile crystals was estimated by metallographic microscope images.

Table 1 Chemical compositions of samples (mass fraction, %)

Sample No.	CaO	SiO_2	TiO_2	Ti_2O_3	Al_2O_3	MgO	FeO	MFe
1	26.87	25.13	17.58	3.86	14.08	7.86	1.51	2.18
2	4.32	8.85	60.72	14.65	2.64	2.02	−	0.96

No. 1: Ti-bearing blast furnace slag; No. 2: Titanium slag

2.3 Characterization

The chemical components of Ti-bearing blast furnace slag, titanium slag, and rutile were analyzed by inductively coupled plasma-atomic emission spectroscopy (ICP−AES, PerkinElmer Optima−4300DV) except for the contents of Ti_2O_3, FeO, and metallic iron (MFe). The Ti_2O_3 content was determined by oxidation−reduction titration. The FeO content was determined by *o*-phenanthroline oxidation−reduction titration, and the metallic iron content was determined by ferric chloride oxidation−potassium dichromate titration. The phase compositions of products were identified by XRD analysis (X'PERT PROMPD/PW3040, PANalytical B.V. Corp., Netherlands) using Cu K_α radiation for 7 min from 10° to 90°. The microscopic observation of samples was conducted by using a scanning electron microscopy (SEM, TESCAN VEGA III). Quenched samples were observed by a metallographic microscope (201A−D) to estimate settling time. The volume fraction and average particle size of rutile crystals were measured on a Quantime520 image analyzer by the line intercept method (average of 15 fields).

3 Results and discussion

3.1 Theoretical analysis for effect of rutile crystal shapes on rutile settlement

The settling velocity of a spherical rutile crystal with diameter (d) was calculated. When the settling velocity is reached, the resistance is equal to the gravity minus the buoyancy.

$$\frac{\pi d^3}{6}(\rho_r-\rho)g=\zeta\frac{\pi d^2}{4}\times\frac{\rho u_0^2}{2} \tag{1}$$

where ρ_r is the density of rutile; ρ is the density of molten slag; g is the gravitational acceleration; ζ is the drag coefficient; u_0 is the settling velocity.

The settling velocity obtained by solving Eq. (1) is

$$u_0=\sqrt{\frac{4d(\rho_r-\rho)g}{3\zeta\rho}} \tag{2}$$

When Reynolds number $Re_0\leq 2$, the equations for calculating drag coefficient and Reynolds number are as follows:

$$\zeta=\frac{24}{Re_0} \tag{3}$$

$$Re_0=\frac{du_0\rho}{\mu} \tag{4}$$

where μ is the viscosity of molten slag.

Substituting Eqs. (3) and (4) into Eq. (2) yields

$$u_0=\frac{gd^2(\rho_r-\rho)}{18\mu} \tag{5}$$

For non-spherical rutile crystal, WADELL [23] conducted related researches. He converted a non-spherical crystal into an equal-volume spherical crystal, and then added a coefficient (k_1) to Eq. (5) to characterize the settling velocity of a non-spherical crystal, and the settling velocity (u_0') is

$$u_0'=k_1\frac{gd^2(\rho_r-\rho)}{18\mu} \tag{6}$$

$$k_1=0.8431\lg(\Phi/0.065) \tag{7}$$

$$\Phi=S_1/S_2 \tag{8}$$

where Φ is the degree of sphericity; S_1 is the spherical volume-equivalent surface area of a crystal; S_2 is the actual surface area of a non-spherical crystal.

Under the same volume conditions, the relationships among the surface areas of spherical (a), cubic (b), and cuboid (c) crystals follow the sequence:

$$S_a<S_b<S_c \tag{9}$$

Therefore,

$$\Phi_c<\Phi_b<\Phi_a=1 \tag{10}$$

Thus,

$$u_a>u_b>u_c \tag{11}$$

In summary, the settling velocity of a spherical rutile crystal is larger than their equivalent ones under the same volume conditions. Thus, spherical shape favors the settlement of rutile crystals in the modified slag.

3.2 Theoretical analysis for effect of TiO_2 content on rutile crystal shapes

When the supersaturated solution was homogeneously nucleated, the Gibbs free energy change (ΔG) mainly includes two parts: the interface energy change (ΔG_s) caused by the formation of a new interface, and the Gibbs free energy change (ΔG_v) caused by a decrease in solution supersaturation.

$$\Delta G=\Delta G_s+\Delta G_v \tag{12}$$

$$\Delta G_{\mathrm{v}}=\frac{4}{3}\pi r^{3}RT\ln(S_{0}/S)\frac{\rho}{M} \tag{13}$$

$$\Delta G_{\mathrm{s}}=4\pi r^{2}\sigma_{\mathrm{s-1}} \tag{14}$$

where r is the radius of rutile crystal; R is gas constant; M is the molar mass of rutile; S_0 is the saturation concentration of big rutile crystal; S is the saturation concentration of small rutile crystal; $\sigma_{\mathrm{s-1}}$ is the interfacial tension between crystal and solution.

Substituting Eqs. (13) and (14) into Eq. (12) to obtain the ΔG:

$$\Delta G=4\pi r^{2}\sigma_{\mathrm{s-1}}+\frac{\frac{4}{3}\pi r^{3}\rho RT\ln(S_{0}/S)}{M} \tag{15}$$

Solving differential equation $\mathrm{d}(\Delta G)/\mathrm{d}r$ and letting $\mathrm{d}(\Delta G)/\mathrm{d}r=0$, the critical radius ($r^*$) of the nucleus is obtained.

$$r^{*}=2\sigma_{\mathrm{s-1}}M/[\rho RT\ln(S/S_{0})] \tag{16}$$

Substituting Eq. (16) into Eq. (15), the expression of $\Delta G_{\max}$ can be obtained. The $\Delta G_{\max}$ is the Gibbs free energy change which is required to form critical nuclei.

$$\Delta G_{\max}=\frac{16\pi\sigma_{\mathrm{s-1}}^{3}M^{2}}{3[\rho RT\ln(S/S_{0})]^{2}} \tag{17}$$

The ratio (J) of homogeneous nucleation can be expressed by the following formula. The k is a proportional constant.

$$J=k\exp[-\Delta G_{\max}/(RT)] \tag{18}$$

Substituting Eq. (17) into Eq. (18), the expression of J can be obtained.

$$J=k\exp\left\{-\frac{16}{3}\frac{\pi\sigma_{\mathrm{s-1}}^{3}M^{2}}{\rho^{2}(RT)^{3}[\ln(S/S_{0})]^{2}}\right\} \tag{19}$$

Therefore, increasing the supersaturation (S/S_0) is beneficial to nucleation. In other words, the rate of rutile crystal nucleation is much greater than that of rutile crystal growth at higher supersaturation. Therefore, the molten slag could generate a large number of rutile crystal nuclei in a short time, resulting in large consumption of titanium oxides, which limits the growth of the rutile crystals, and thereby promoting the shape transformation of rutile crystals into sphere. In the present study, the supersaturation of the molten slag can be increased by increasing the titanium oxides content in the raw materials, i.e., adding titanium slag to Ti-bearing blast furnace slag.

3.3 Formation mechanism of rutile

To study the formation mechanism of rutile, the standard Gibbs free energy changes of Reactions (1)−(10) were calculated by FactSage. The results are shown in Fig. 1.

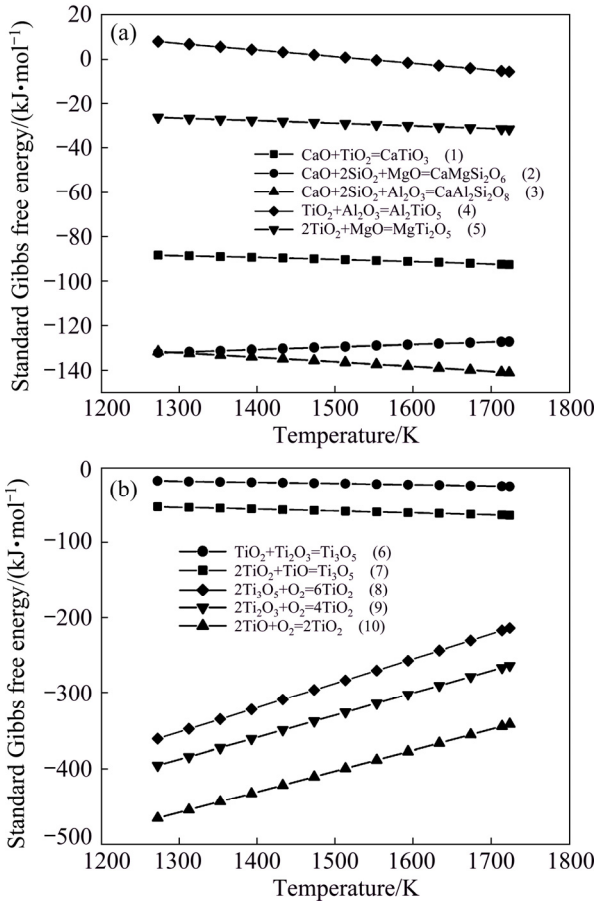

Fig. 1 Standard Gibbs free energy changes of reactions: (a) Reactions (1)–(5); (b) Reactions (6)–(10)

It is well known that the molecular formula of anosovite can be represented by $(DO\cdot 2TiO_2)_m\cdot(E_2O_3\cdot TiO_2)_n$. In this work, DO is divalent oxides mainly including MgO and TiO, and E_2O_3 is trivalent oxides mainly containing Al_2O_3 and Ti_2O_3. Thus, the precipitation reactions of anosovite can be expressed by Reactions (4)−(7). As shown in Fig. 1(a), the standard Gibbs free energies of Reactions (2) and (3) are less than those of Reactions (1), (4) and (5), implying that Reactions (1), (4) and (5) are inhibited with the added SiO_2, i.e., the precipitation of anosovite and perovskite is restrained. Therefore, Ti components can only exist in form of simple titanium oxides, such as TiO, Ti_2O_3, Ti_3O_5, and TiO_2. As shown in Fig. 1(b), the standard Gibbs free energies of Reactions (8)−(10) are less than those of Reactions

(6) and (7), indicating that Reactions (6) and (7) are inhibited with the added O_2, i.e., the precipitation of anosovite is restrained. Hence, Ti components are present as TiO_2.

In summary, when O_2 and SiO_2 are simultaneously added to the modified slag, it can be seen from Fig. 1 that Reactions (1) and (4)−(7) are inhibited and Ti components can only exist in form of TiO_2. Therefore, TiO_2 converts into rutile at a high temperature.

3.4 FactSage simulation

The scheme of FactSage simulation is listed in Table 2, and the results of FactSage simulation are shown in Fig. 2.

It was found from Table 2 (No. a) and Fig. 2(a) that the mass of rutile precipitates increased significantly as the added O_2 increased from 5 to 20 g. As the added O_2 continuously increased to 35 g, the rutile precipitates almost remained unchanged. Thus, the optimal added O_2 was 20 g. As shown in Table 2 (No. b) and Fig. 2(b), when the added SiO_2 is in the range of 30−90 g, the rutile precipitates increased rapidly. When the added SiO_2 was higher than 90 g, the rutile precipitates were almost constant. Therefore, the optimal SiO_2 was 90 g. As illustrated in Table 2 (No. c) and Fig. 2(c), when the added O_2 increased from 5 to 20 g, the rutile precipitates increased significantly. As for the case of the O_2 addition more than 20 g, the rutile precipitates remained unchanged. Thus, the optimal added O_2 was 20 g. It can be seen from Table 2 (No. d) and Fig. 2(d), that the rutile precipitates dramatically increased with the added SiO_2 increasing from 10 to 50 g. Thereafter, in the SiO_2 addition range of 50−70 g, the rutile precipitates were nearly constant. Thus, the optimal added SiO_2 was 50 g. As shown in Table 2 (No. e) and Fig. 2(e), the rutile precipitates dramatically increased as the added O_2 increased from 5 to 15 g. Nevertheless, the rutile precipitates remained unchanged with the addition of 15−25 g O_2. Therefore, the optimum added O_2 was 15 g. As illustrated in Table 2 (No. f) and Fig. 2(f), the rutile precipitates rapidly increased from 10 to 40 g, and remained unchanged with more than 40 g. Therefore, the optimal SiO_2 was 40 g.

3.5 Demonstration of modification experiments

3.5.1 Laboratory experiments

To verify the validity of the aforementioned theoretical analysis, related experiments were carried out. The specific experimental program is provided in Table 3. The SEM images of the upper and lower parts of the modified slag are shown in Fig. 3. The volume fraction and particle size of the rutile crystals in the upper and lower parts of the modified slag are shown in Fig. 4.

As shown in Figs. 3(a), 3(b) and 4(a), for experimental program 1 (Table 3), the volume fractions of the rutile crystals in the upper and lower parts of the modified slag were 33% and 35%, respectively, which implies that rutile settlement barely occurs. For the experimental program 2 (Table 3), the volume fractions of the rutile crystals in the upper and lower parts of the modified slag were 31% and 45%, respectively, indicating that the occurrence of rutile settlement. For experimental program 3 (Table 3), the volume fractions of the rutile crystals in the upper and lower parts of the modified slag were 30% and 71%, respectively, implying that rutile settlement was obvious. As shown in Figs. 3(b), (d) and (f), with the increase of titanium oxides in the raw materials, the shapes of rutile crystals transformed from rod to sphere. The results evidenced the authenticity of the theoretical analysis in Sections 3.1 and 3.2, i.e., the increase of titanium oxides in the raw materials can promote the conversion of rutile crystals from rod into sphere, thereby achieving the settlement of

Table 2 Scheme of FactSage simulation

No.	Fixed condition	Addition	Optimal mass/g
a	Ti-bearing blast furnace slag 407 g, titanium slag 93 g, SiO_2 90 g	O_2	20
b	Ti-bearing blast furnace slag 407 g, titanium slag 93 g, O_2 20 g	SiO_2	90
c	Ti-bearing blast furnace slag 315 g, titanium slag 185 g, SiO_2 50 g	O_2	20
d	Ti-bearing blast furnace slag 315 g, titanium slag 185 g, O_2 20 g	SiO_2	50
e	Ti-bearing blast furnace slag 222 g, titanium slag 278 g, SiO_2 40 g	O_2	15
f	Ti-bearing blast furnace slag 222 g, titanium slag 278 g, O_2 15 g	SiO_2	40

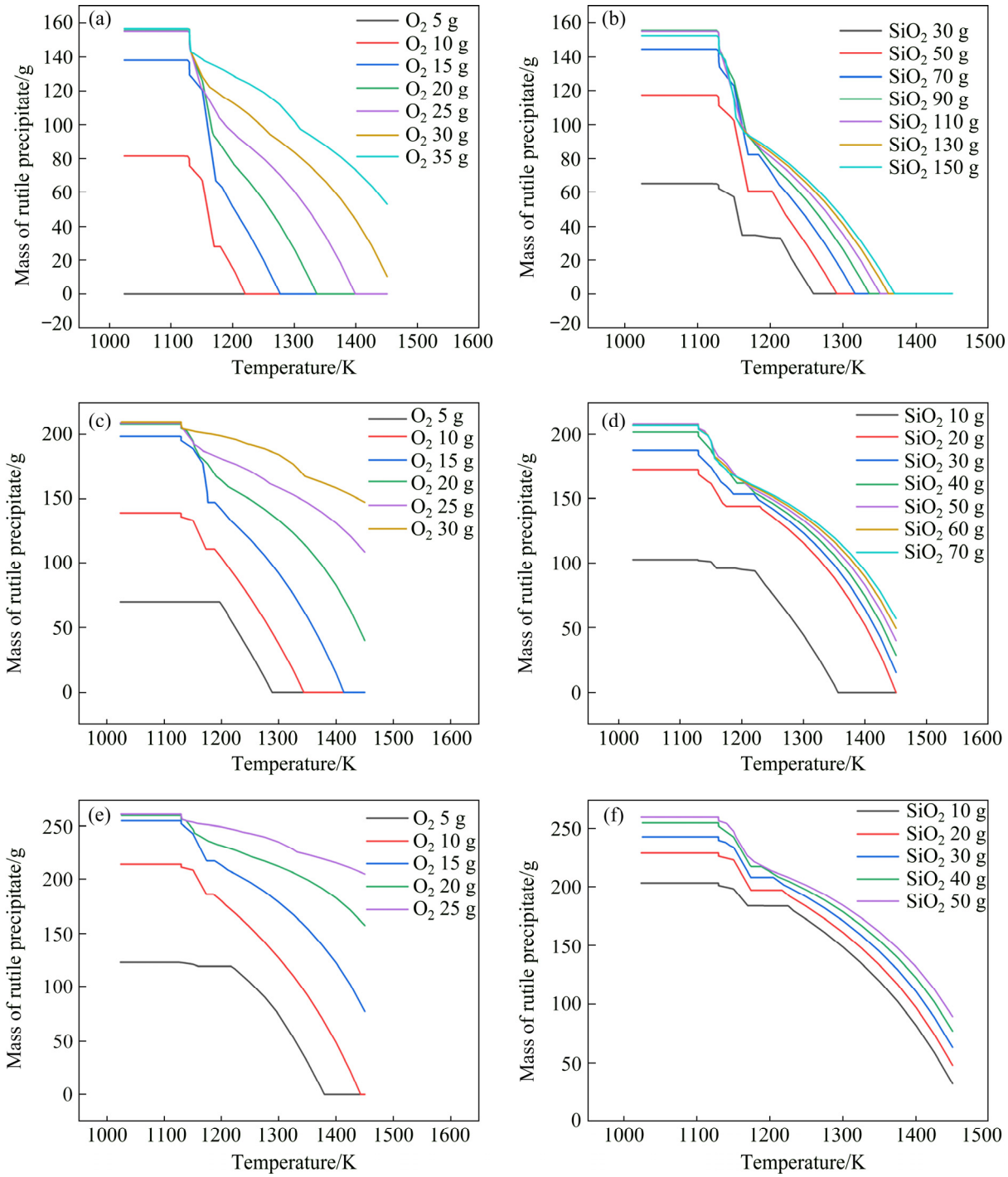

Fig. 2 Relationships among added O_2, SiO_2 and rutile precipitates corresponding with (a−f) in Table 2, respectively

Table 3 Experimental program and parameters

No.	Mass/g			
	Ti-bearing blast furnace slag	Titanium slag	SiO_2	O_2
1	407	93	90	20
2	315	185	50	20
3	222	278	40	15
4	44400	55600	8000	3000

rutile crystals. LI et al [15] and DU et al [20,21] conducted related researches on the selective precipitation and separation of rutile from Ti-bearing blast furnace slag, and they found that rutile crystals are rod-shaped. But the rutile crystals in this work are spherical. The reason for this difference is that the content of titanium oxides of the raw materials (47%) in this study is much higher than that (22%) in the above literatures.

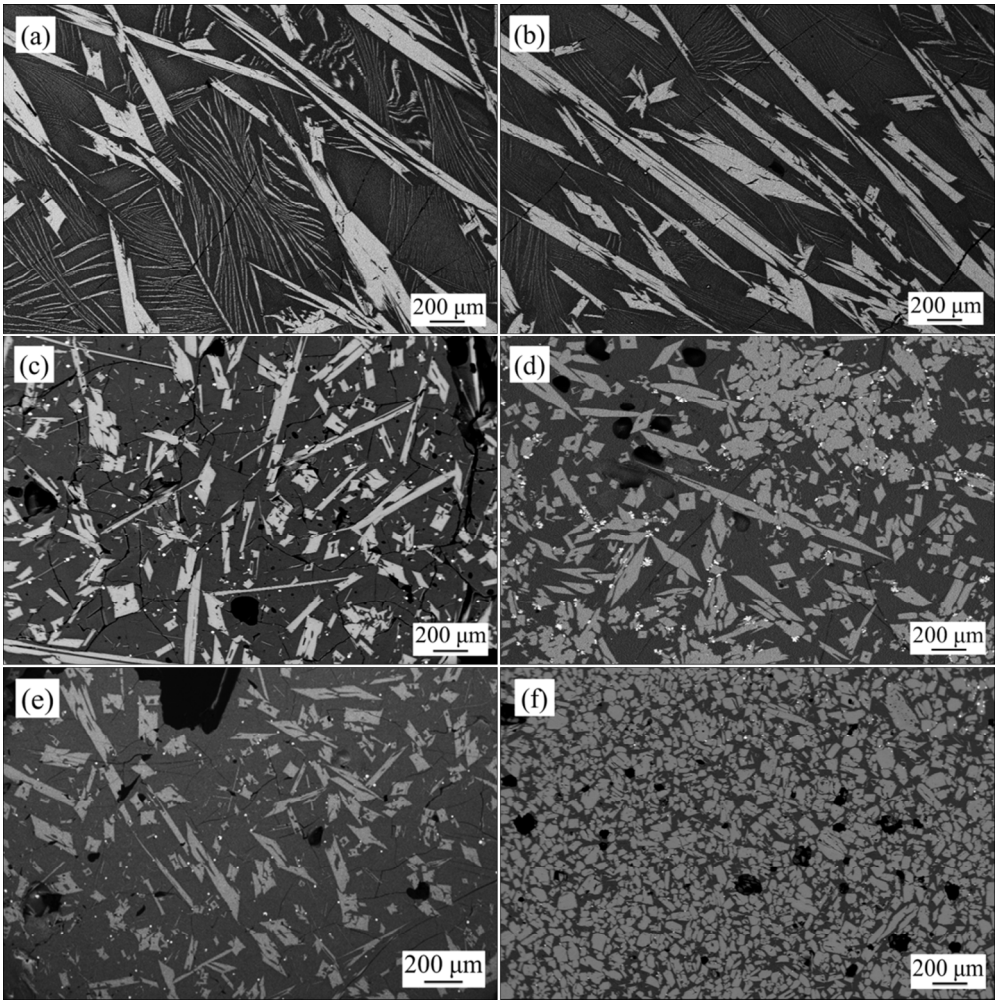

Fig. 3 SEM images of upper (a, c, e) and lower (b, d, f) parts of modified slag for No.1 (a, b), No. 2 (c, d) and No. 3 (e, f) in Table 3, respectively

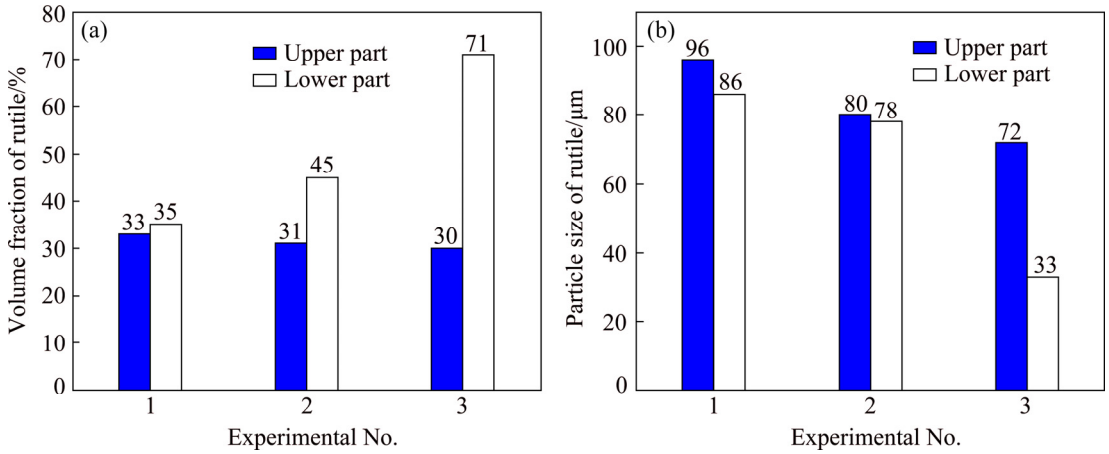

Fig. 4 Volume fraction (a) and particle size (b) of rutile crystals in upper and lower parts of modified slag under different experimental schemes in Table 3

Based on the results shown in Fig. 4(b), with the increase of titanium oxides in the raw materials, the average particle size of rutile crystals gradually reduced. This is because an increased supersaturation favors the nucleation of rutile crystals, thereby limiting the growth of rutile crystals. This further proves the validity of the theoretical analysis of Section 3.2.

3.5.2 Pilot experiments

As shown in Table 3 (No. 4), the optimal conditions of laboratory experiments (No. 3) were magnified 200× for pilot experiments. The picture of the modified slag, the SEM images of rutile settlement, and their corresponding volume fraction and average particle size of rutile crystals in different positions are shown in Figs. 5, 6, and 7, respectively. The XRD patterns and chemical compositions of the upper and lower parts in the modified slag are shown in Fig. 8 and Table 4, respectively. The metallographic microscope images of the quenched samples after cooling for 6, 10, 14, and 18 min are shown in Fig. 9, and the relationship between settling time and the volume fraction of rutile is shown in Fig. 10.

As shown in Figs. 5 and 6, the height of the modified slag was 46 cm, and we took samples vertically with an interval of 11.5 cm from the top center of the slag to the bottom center. As shown in Figs. 6 and 7(a), the volume fraction of rutile crystals in the upper part of the slag was 31%−40%, and the corresponding volume fraction of rutile crystals in the lower part of the slag was 72%−75%. As shown in Table 4, the TiO_2 contents in the upper and lower parts of the modified slag were 28.21% and 70.53%, respectively, which indicates a strong

Fig. 5 Picture of modified slag

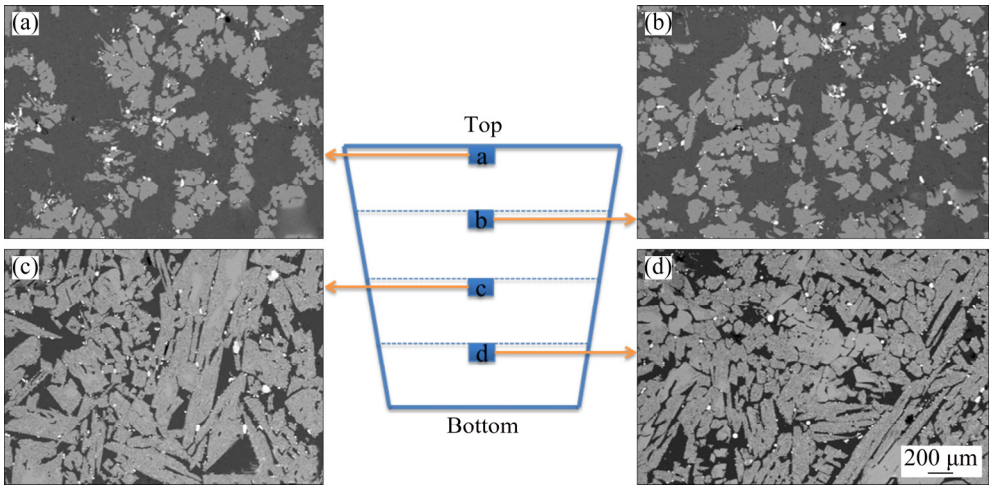

Fig. 6 SEM images of rutile settlement in different positions

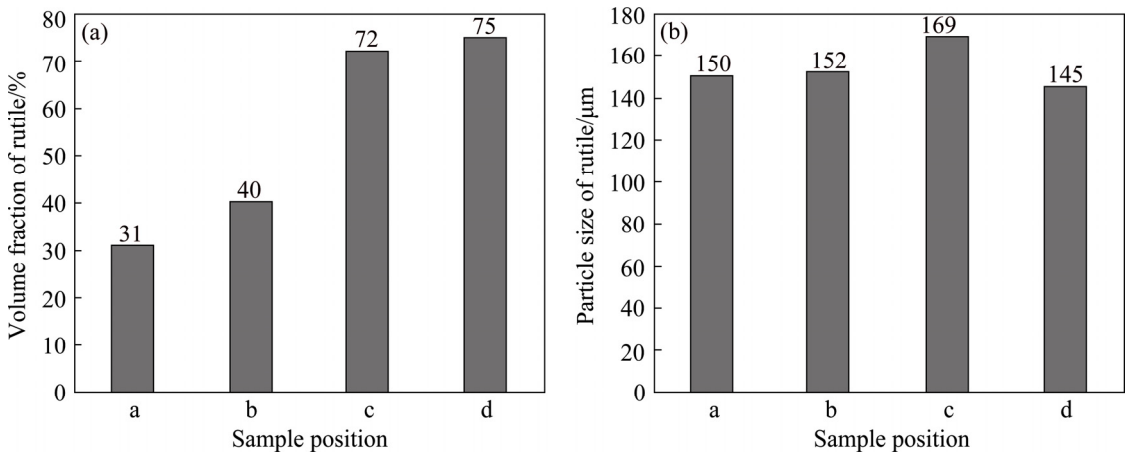

Fig. 7 Volume fraction (a) and average particle size (b) of rutile crystals in different positions of modified slag in Fig. 6

indication of efficient settlement of rutile crystals. As shown in Figs. 4(b) and 7(b), the average particle sizes of the rutile crystals in the modified slag obtained from laboratory and pilot experiments were 33−72 and 145−169 μm, respectively. This indicates that larger scale of experiments were conducive to the growth of rutile crystals; the larger the experimental scale, the smaller the cooling rate of the modified slag, which was more beneficial to the growth of rutile crystals.

As shown in Fig. 8, the modified slag contained only rutile. It can be seen from Fig. 6 that the modified slag contained two phases, i.e., rutile and gangue. Thus, it can be concluded that the gangue was glass phase. Furthermore, the modified slag contained only rutile and glass phase, indicating that the raw materials were almost completely melted at 1450 °C. On one hand, the addition of O_2 oxidized the high melting point substances (TiC, TiN, and the low-value titanium oxides), and thereby decreased the melting point of the slag. On the other hand, the addition of SiO_2 promoted the conversion of perovskite and spinel into low melting point substances, as a consequence, the melting point of the slag was reduced.

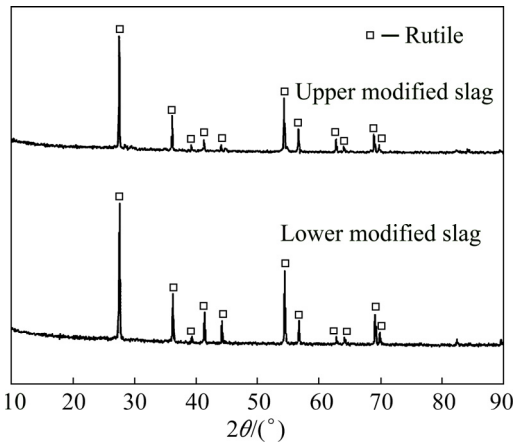

Fig. 8 XRD patterns of upper and lower parts in modified slag

Table 4 Chemical compositions of upper (U) and lower (L) parts in modified slag (mass fraction, %)

Sample	TiO_2	SiO_2	CaO	Al_2O_3	MgO	Fe_2O_3
U	28.21	31.02	18.23	9.34	5.41	4.87
L	70.53	12.49	7.38	3.95	2.52	1.22

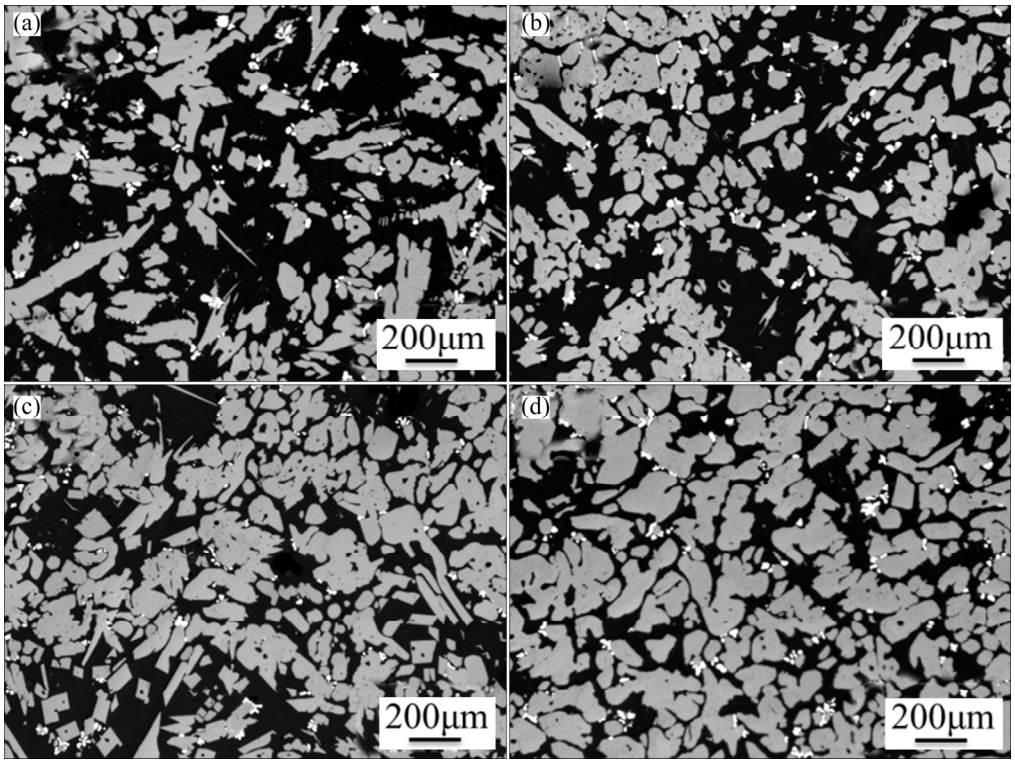

Fig. 9 Metallographic microscope images of quenched samples after cooling for 6 min (a), 10 min (b), 14 min (c) and 18 min (d)

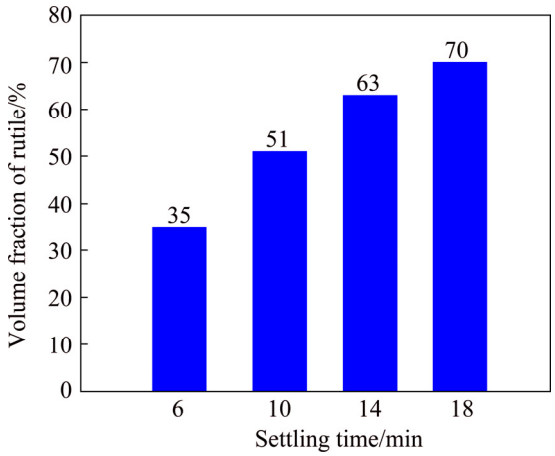

Fig. 10 Relationship between settling time and volume fraction of rutile

As shown in Figs. 9 and 10, the volume fraction of rutile increased as settling time prolonged. When settling time was 18 min, the volume fraction of rutile increased to maximum (70%). Thus, the actual settling time of rutile crystals was about 18 min. The theoretical settling velocities of rutile crystals were calculated by Formula (5). Here, g is 10 m/s^2; d is 150 μm; ρ_r is 4300 kg/m^3; ρ is the density of molten slag (2800 kg/m^3); μ is the viscosity of molten slag at 1450 °C (0.013 Pa·s). So, u_0 is calculated as 0.0014 m/s. If the depth of molten slag is 0.5 m, the theoretical settling time of rutile crystals is 6 min. The reason why the actual settling time is much larger than the theoretical settling time is that the theoretical time ignores the interaction forces between the rutile crystals.

3.6 Selective separation of rutile in pilot experiments

According to the flow chart (Fig. 11), high-quality rutile could be obtained from the upper part in the modified slag by combination of shaker sorting and hydrochloric acid leaching. The optimal parameters of shaker sorting process are: particle size around 150 μm, stroke 12 mm, vibration frequency 360 times/min, and inclination angle 1°. The optimum conditions of hydrochloric acid leaching process are: particle size around 150 μm, hydrochloric acid concentration 15% (volume fraction), leaching temperature 65 °C, leaching time 3 h, and a liquid-to-solid ratio of 3. Based on the flow chart, high-quality rutile was also obtained from the lower part in the modified slag by hydrochloric acid leaching under the following optimum conditions: particle size about 150 μm, hydrochloric acid concentration 15% (volume fraction), leaching temperature 65 °C, leaching time 3 h, and a liquid-to-solid ratio of 3.

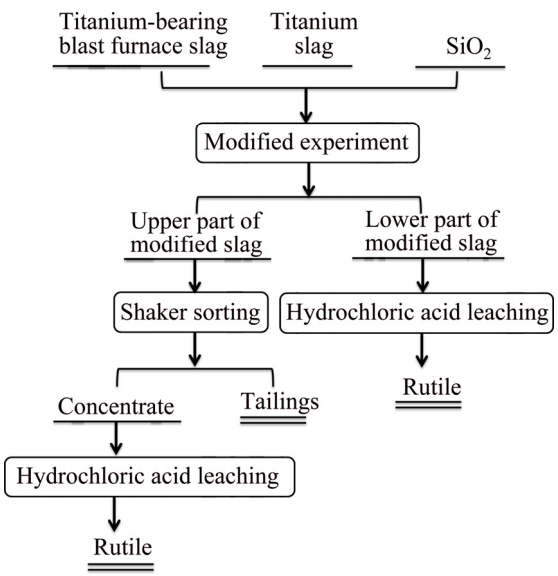

Fig. 11 Flow chart for preparation of rutile

The XRD patterns and chemical compositions of the rutile obtained from the upper part of the modified slag by shaker sorting-hydrochloric acid leaching and the lower part in the modified slag by hydrochloric acid leaching are shown in Fig. 12 and Table 5. The TiO_2 recovery rates and mass fractions of the upper and lower parts in the modified slag under different treatment processes are provided in Table 6, and the calculation formulas of TiO_2 recovery rates are as follows:

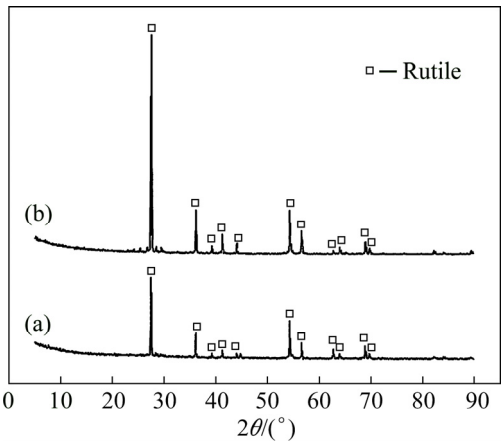

Fig. 12 XRD patterns of rutile: (a) Rutile obtained from upper part in modified slag by shaker sorting−hydrochloric acid leaching; (b) Rutile obtained from lower part in modified slag by hydrochloric acid leaching

$$\eta_S = \frac{w_S m_S}{500w} \times 100\% \tag{20}$$

$$\eta_H = \frac{w_H m_H}{100w_S} \times 100\% \tag{21}$$

$$\eta_T = \eta_S \eta_H \tag{22}$$

where w is the TiO_2 content of the modified slag; w_S is the TiO_2 content of product after shaker sorting; m_S is the mass of product after shaker sorting; η_S is the recovery rate of TiO_2 after shaker sorting; w_H is the TiO_2 content of product after hydrochloric acid leaching; m_H is the mass of product after hydrochloric acid leaching; η_H is the recovery rate of TiO_2 after hydrochloric acid leaching; η_T is the total recovery rate of TiO_2; 500 denotes the mass of the raw material in shaker sorting (g); 100 denotes the mass of the raw material in hydrochloric acid leaching (g).

As shown in Fig. 12, the products obtained from the upper part of the modified slag by shaker sorting−hydrochloric acid leaching and the lower part of the modified slag by hydrochloric acid leaching are all rutile. As illustrated in Table 5, the TiO_2 contents of the rutile obtained from the upper part of the modified slag by shaker sorting−hydrochloric acid leaching and the lower part of the modified slag by hydrochloric acid leaching were greater than 93%. Further, their total contents of CaO and MgO were all not higher than 0.4%, meeting the requirements for the raw materials of titanium white synthesis with the chloride process.

As shown in Table 6, the recovery rate of TiO_2 in the upper part of the modified slag is only 73.07%, which is caused by the low recovery rate of TiO_2 in shaker sorting process. In contrast, the recovery rate of TiO_2 in the lower part of the modified slag is up to 98.74%, as the lower part of the modified slag can be directly leached by hydrochloric acid to obtain high-quality rutile (due to rutile settlement), thereby eliminating the shaker sorting process and increasing the recovery rate of TiO_2.

4 Conclusions

(1) The settling velocities of spherical rutile crystals are faster than those of other shapes of rutile crystals under the same volume conditions.

(2) The shape transformation of rutile crystals from rod to sphere can be achieved by adding titanium slag to Ti-bearing blast furnace slag.

(3) The volume fractions of the rutile crystals in the upper and lower parts of the modified slag are 30% and 71% when the added titanium slag increases to 278 g, indicating an obvious settlement of rutile.

(4) The settlement of rutile crystals can save half the shaker sorting task for the technology and significantly increase the recovery rate of TiO_2.

(5) The TiO_2 content of the rutile, obtained from the upper part of the modified slag by shaker sorting−hydrochloric acid leaching, is 93.03%, and the corresponding total content of CaO and MgO is 0.40%.

(6) The TiO_2 content of the rutile, obtained from the lower part of the modified slag by hydrochloric acid leaching, is 96.11%, and the corresponding total content of CaO and MgO is 0.22%.

Table 5 Chemical compositions of rutile (mass fraction, %)

Sample No.	TiO_2	SiO_2	Al_2O_3	Fe_2O_3	MgO	CaO	MnO	P_2O_5	SO_3
1	93.03	3.55	1.36	0.72	0.30	0.10	0.08	<0.01	<0.01
2	96.11	1.64	0.80	0.50	0.17	0.05	0.03	<0.01	<0.01

No. 1—Rutile obtained from upper part in modified slag by shaker sorting−hydrochloric acid leaching; No. 2—Rutile obtained from lower part in modified slag by hydrochloric acid leaching

Table 6 Recovery rates and mass fractions of TiO_2 of samples under different treatment processes

Sample	w/%	w_S/%	η_S/%	w_H/%	η_H/%	η_T/%
Upper	28.21	62.43	74.35	93.03	98.28	73.07
Lower	70.51	−	−	96.11	98.74	98.74

References

[1] DU He-gui. Theory of smelting V and Ti-magnetite by blast furnace [M]. Beijing: Science Press, 1996. (in Chinese)

[2] FENG Cong, GAO Li-hua, TANG Jue, LIU Zheng-gen, CHU Man-sheng. Effects of MgO/Al_2O_3 ratio on viscous behaviors and structures of $MgO-Al_2O_3-TiO_2-CaO-SiO_2$ slag systems with high TiO_2 content and low CaO/SiO_2 ratio [J]. Transactions of Nonferrous Metals Society of China, 2020, 30(3): 800−811.

[3] WANG Shuai, GUO Yu-feng, ZHENG Fu-qiang, CHEN Feng, YANG Ling-zhi, JIANG Tao, QIU Guan-zhou. Behavior of vanadium during reduction and smelting of vanadium titanomagnetite metallized pellets [J]. Transactions of Nonferrous Metals Society of China, 2020, 30(6): 1687−1696.

[4] LI Liao-sha, SUI Zhi-tong. Physical chemistry behavior of enrichment selectivity of TiO_2 in perovskite [J]. Acta Physico-Chimica Sinica, 2001, 17(9): 845−849. (in Chinese)

[5] LI Liao-sha, LOU Tai-ping, CHE Chang-yin, SUI Zhi-tong. Kinetics on the oxidation of $CaO-SiO_2-Al_2O_3-MgO-TiO_x-FeO_y$ system [J]. Acta Physico-Chimica Sinica, 2000, 16(8): 708−712. (in Chinese)

[6] WANG Xi-dong, MAO Yu-wen, LIU Xiang-ying, ZHU Yuan-kai. Study on crystallization behavior of blast furnace slag containing TiO_2 [J]. Journal of Iron and Steel Research, 1990, 2(3): 1−6. (in Chinese)

[7] WANG Ming-yu, WANG Xue-wen, HE Yue-hui, LOU Tai-ping, SUI Zhi-tong. Isothermal precipitation and growth process of perovskite phase in oxidized titanium bearing slag [J]. Transactions of Nonferrous Metals Society of China, 2008, 18(2): 459−462.

[8] ZHANG Li, ZHANG Lin-nan, WANG Ming-yu, LOU Tai-ping, SUI Zhi-tong, JANG Jing-shi. Effect of perovskite phase precipitation on viscosity of Ti-bearing blast furnace slag under the dynamic oxidation condition [J]. Journal of Non-Crystalline Solids, 2006, 352(2): 123−129.

[9] ZHANG Li, ZHANG Lin-nan, WANG Ming-yu, LI Guang-qiang, SUI Zhi-tong. Precipitation selectivity of perovskite phase from Ti-bearing blast furnace slag under dynamic oxidation conditions [J]. Journal of Non-Crystalline Solids, 2007, 353(22−23): 2214−2220.

[10] ZHANG Li, ZHANG Lin-nan, WANG Ming-yu, LI Guang-qiang, SUI Zhi-tong. Recovery of titanium compounds from molten Ti-bearing blast furnace slag under the dynamic oxidation condition [J]. Minerals Engineering, 2007, 20(7): 684−693.

[11] SUI Zhi-tong, ZHANG Peng-xing, YAMAUCHI C. Precipitation selectivity of boron compounds from slags [J]. Acta Materialia, 1999, 47(4): 1337−1344.

[12] WANG Ming-yu, LI Liao-sha, ZHANG Li, ZHANG Lin-nan, TU Gan-feng, SUI Zhi-tong. Effect of oxidization on enrichment behavior of TiO_2 in titanium-bearing slag [J]. Rare Metals, 2006, 25(2): 106−110.

[13] WANG Ming-yu, ZHANG Lin-nan, ZHANG Li, SUI Zhi-tong, TU Gan-feng. Selective enrichment of TiO_2 and precipitation behavior of perovskite phase in titania bearing slag [J]. Transactions of Nonferrous Metals Society of China, 2006, 16(2): 421−425.

[14] ZHANG Li, ZHANG Wu, ZHANG Ju-hau, LI Guang-qiang. Effects of additives on the phase transformation, occurrence state, and the interface of the ti component in ti-bearing blast furnace slag [J]. International Journal of Minerals Metallurgy and Materials, 2016, 23(9): 1029−1040.

[15] LI Jing, WANG Xi-dong, ZHANG Zuo-tai. Crystallization behavior of rutile in the synthesized Ti-bearing blast furnace slag using single hot thermocouple technique [J]. ISIJ International, 2011, 51(9): 1396−1402.

[16] SUN Yong-qi, LI Jing, WANG Xi-dong, ZHANG Zuo-tai. The effect of P_2O_5 on the crystallization behaviors of Ti-bearing blast furnace slags using single hot thermocouple technique [J]. Metallurgical and Materials Transactions B, 2014, 45(4): 1446−1455.

[17] ZHANG Wu, ZHANG Li, ZHANG Ju-hua, FENG Nai-xiang. Crystallization and coarsening kinetics of rutile phase in modified Ti-bearing blast furnace slag [J]. Industrial & Engineering Chemistry Research, 2012, 51(38): 12294−12298.

[18] ZHANG Li, ZHANG Ju-hua, ZHANG Wu, LI Guang-qiang. Thermodynamic analysis of extraction of synthetic rutile from modified slag [J]. Industrial & Engineering Chemistry Research, 2013, 52(13): 4924−4931.

[19] ZHANG Li, LI Guang-qiang, ZHANG Wu. Synthesis of rutile from high titania slag by pyrometallurgical route [J]. Transactions of Nonferrous Metals Society of China, 2011, 21(10): 2317−2322.

[20] DU Yu, GAO Jin-tao, LAN Xi, GUO Zhan-cheng. Recovery of rutile from Ti-bearing blast furnace slag through phase transformation and super-gravity separation for dielectric material [J]. Ceramics International, 2020, 46(7): 9885−9893.

[21] DU Yu, GAO Jin-tao, LAN Xi, GUO Zhan-cheng. Selective precipitation and in-situ separation of rutile crystals from titanium bearing slag melt in a super-gravity field [J]. Cryst Eng Comm, 2018, 20(27): 3868−3876.

[22] HAN Ji-qing, ZHANG Jing, FENG Wei, CHEN Xiao, ZHANG Li, TU Gan-feng. A Clean process to prepare high-quality acid-soluble titanium slag from titanium middling ore [J]. Minerals, 2019, 9(8): 460.

[23] WADELL H. The coefficient of resistance as a function of Reynolds number for solids of various shapes [J]. Journal of the Franklin Institute, 1934, 217(4): 459−490.

金红石晶体形状对其沉降的影响

韩吉庆[1]，张家豪[1]，陈 晓[2]，张 晶[1]，张 力[1]，涂赣峰[1]

1. 东北大学 冶金学院，沈阳 110819；
2. 东北大学 材料科学与工程学院， 沈阳 110819

摘 要：通过理论分析、FactSage 模拟、XRD 和 SEM，研究金红石晶体形状对其在改性渣中沉降的影响。结果表明，在相同体积条件下，球状金红石晶体的沉降速度大于其他形状金红石晶体的沉降速度；通过向含钛高炉渣中添加钛渣可以实现金红石晶体由棒状向球状的转变；当钛渣的添加量增加至 278 g 时，改性渣上部和下部金红石晶体的体积分数分别为 30%和 71%，说明金红石沉降明显。由于金红石的沉降，节省了 50%的重选任务，且显著增加了 TiO_2 的回收率。产品金红石中 TiO_2 含量高于 93%，CaO 和 MgO 的总含量低于 0.4%，满足氯化法钛白对原料的要求。

关键词：金红石晶体形状；含钛高炉渣；钛渣；改性；重选；酸浸

(Edited by Xiang-qun LI)